JGR Space Physics

RESEARCH ARTICLE
10.1029/2021JA029329

Association of Auroral Streamers and Bursty Bulk Flows During Different States of the Magnetotail: A Case Study

Banafsheh Ferdousi[1], Joachim Raeder[1], Eftyhia Zesta[2], William Cramer[1], and Kyle Murphy[3]

[1]Department of Physics and EOS Space Science Center, University of New Hampshire, Durham, NH, USA, [2]NASA Goddard Space Flight Center, Greenbelt, MD, USA, [3]Department of Astronomy, University of Maryland, College Park, MD, USA

Key Points:

- Mapped fast flows from the magnetosphere to the ionosphere resemble auroral streamers in the simulation
- The number of fast flows and streamer increases during substorm expansion and SMC, and they penetrate closer to the Earth during SMC
- The location of BBFs is controlled by the state of the magnetosphere and interplanetary magnetic field (IMF) B_y

Supporting Information:

Supporting Information may be found in the online version of this article.

Correspondence to:

B. Ferdousi,
banafsheh.ferdousi@unh.edu

Citation:

Ferdousi, B., Raeder, J., Zesta, E., Cramer, W., & Murphy, K. (2021). Association of auroral streamers and bursty bulk flows during different states of the magnetotail: A case study. *Journal of Geophysical Research: Space Physics*, *126*, e2021JA029329. https://doi.org/10.1029/2021JA029329

Received 16 MAR 2021
Accepted 1 SEP 2021

Abstract In-situ measurements in the magnetotail are sparse and limited to single points. On the other hand, there is a broad range of observations, including magnetometers, aurora imagers, and radars, in the ionosphere. Since the nightside ionosphere resembles the magnetotail plasma sheet dynamics projection, it can be used to monitor the tail's dynamics. A proper interpretation of the ionosphere and ground observations necessitates understanding the coupling processes between the ionosphere and the magnetosphere. Here, we use the global magnetohydrodynamic simulation model, OpenGGCM-CTIM-RCM, to investigate these coupling processes during periods when the magnetic flux is transported through the tail via narrow fast flow channels, typically called bursty bulk flows (BBFs). We consider three relevant states of the magnetotail: immediately before the substorm's onset, during the expansion of the substorm, and during a steady magnetic convection (SMC) event. The number of flow channels increases, and they penetrate closer to the Earth during SMC. The IMF B_y direction influences fast flows' location but not their orientation in the plasma sheet during this event. However, the dimension of fast flows and streamers do not depend on the IMF conditions and state of the magnetosphere.

1. Introduction

The magnetosphere and ionosphere are connected electromagnetically through a complex system of currents that flow along magnetic field lines. This connection maps the entire volume of the magnetotail within the nightside auroral region at ionospheric altitudes. The magnetotail complex dynamics generate unique signatures in the ionosphere via field-aligned currents (FACs) and particle precipitation. The most distinctive signature of magnetotail activity in the ionosphere is the substorm phenomenon that releases large amounts of magnetic flux from the tail and injects energy to the ionosphere. Poleward boundary intensifications (PBIs) and streamers are more localized signatures of the tail activities in the ionosphere. PBIs are identified as intense and transient auroral intensification initiated around the magnetic separatrix. The streamers are north-south (N-S) aligned auroral features that are often observed on the night-side, and they are associated with enhanced earthward flows or bursty bulk flows (BBFs) in the plasma sheet (Fairfield et al., 1999; Gallardo-Lacourt et al., 2014; Henderson et al., 1998; Ieda et al., 1998; Kauristie et al., 2000; Lyons et al., 2010; Sergeev et al., 1999; Zesta et al., 2000, 2006).

BBFs are short lived, high speed plasma flows that play an important role in the magnetosphere dynamics transferring 60%–100% of the energy, mass, and magnetic flux in the magnetotail (Angelopoulos et al., 1994; Baumjohann & Paschemann, 1990). They are mostly observed in central plasma sheet (CPS) and plasma sheet boundary layer and their occurrence rate in CPS increases with geomagnetic activity when AE index increases (Baumjohann & Paschemann, 1990). Juusola, Østgaard, Tanskanen, Partamies, et al. (2011) also showed that frequency rate of fast Earthward flows depends on different states of substorms and flow speed, and their frequency increases for medium speed flows (100 km/s ≤ V ≤ 500 km/s) during substorm onset and toward the end of substorm growth phase and decrease during substorm recovery phase. However, the frequency of higher speed flows (V ≥ 500 km/s) do not increase during substorm growth phase and onset. Fast flows are mainly observed in the midnight region (Baumjohann & Paschemann, 1990), but Kissinger et al. (2012) has shown that their more diverted to the flanks during steady magnetic convection (SMC). The fast flows direction and location is also influenced by IMF B_y variations (Juusola, Østgaard, & Tanskanen, 2011; Pitkänen et al., 2013, 2019, 2018) showed that BBFs are deflected dawnward

during positive IMF B_y, whereas they are more dusk-ward during negative IMF B_y consistent with Pitkänen et al. (2013) study.

The BBFs have also been interpreted as plasma bubbles, which are magnetic flux tubes whose entropy content is low compared to the surrounding field (Pontius Jr. & Wolf, 1990). As a flux tube of lower entropy content moves earthward, the flow shear between the bubble and its surrounding plasma generates magnetic shear that is associated to FACs, similar to the substorm current wedge polarity, that is, earthward on the dawnside and tailward on the duskside (Kauristie et al., 2000; Keiling et al., 2009; Pontius Jr. & Wolf, 1990). However, the streamers' current wedges are more localized than the substorm current wedge (Zesta et al., 2011). Electron precipitation associated with the upward flowing FAC leads to the formation of streamers in the ionosphere, and the coupling processes result in the auroral signature of BBFs (Kepko et al., 2009; Liang et al., 2011; Mella et al., 2011).

Although the spatial scale of BBFs is difficult to measure directly, Sharma et al. (2008) estimated the length of them to range between $4-40R_E$ and have cross-tail scale of $2-4R_E$ corresponding to their ionospheric counterparts, with approximately one hour magnetic local time (MLT) width. They are also short-lived with a temporal resolution of several minutes, comparable with the temporal scale of streamers (Sergeev et al., 2004). Gabrielse et al. (2018) showed that the average auroral oval flow width is 146 ± 59 km (1.5° in MLT), and their size do not show dependence on season or activity level.

The mesoscale auroral structures are an important part of ionospheric plasma dynamics. They have been suggested as a cause of Space Weather disturbances like the triggering the onset of the substorm caused by the intrusion of north-south streamers into the auroral oval (Lyons et al., 2010; Nishimura et al., 2010). However, this theory is still debated (Frey, 2010; Mende et al., 2011; McPherron et al., 2020).

It is important to understand how these streamers map to fast flows in the plasma sheet. In Sergeev et al. (1999), Figure 3, it is illustrated that auroral streamers map to stretched multi-flow channels in the tail based on Interball-Auroral and Geotail spacecraft. Zesta et al. (2006) also studied the relation between PBIs and fast flows during the expansion and recovery phase of a substorm based on the IMAGE spacecraft FUV auroral imager and Geotail observation in the magnetotail. They used the Tsyganenko (1996) (T96) model to project PBI structures from the ionosphere to the plasma sheet and found that most PBIs map to radially stretched flow channels with no dawnward orientation. However, the resultant configuration may not represent any instantaneous state of the tail because the T96 tail configuration is determined based on averaged magnetic field values. Zesta et al. (2006) also acknowledges that projecting PBIs to the tail using T96 might not be accurate because T96 can yield unreliable results when the magnetic field is highly stretched or changing rapidly. Thus, there is a need to study the magnetotail configuration and PBIs using physics-based self-consistent magnetohydrodynamic (MHD) simulation models to understand the physical processes and conditions that create these magnetotail dynamic structures within the magnetotail's global context and when driven by realistic solar wind conditions.

We build on Zesta et al. (2006) study, which showed that multiple fast flows exist simultaneously across the width of the magnetotail mapping to auroral streamers and PBIs. This study uses the global MHD simulation model coupled to the inner magnetosphere model and coupled thermosphere and ionosphere models to further study the relationship between fast flows and auroral streamers. Because the ionosphere's resolution in the coupled thermosphere ionosphere model cannot resolve the narrow auroral streamers, we map flow channels from the plasma sheet to the ionosphere along field lines to identify the auroral locations and structure. Such mapping based on self-consistent physics-based global models facilitates the study of streamers' source in the magnetotail regardless of their loss during the Magnetosphere-Ionosphere (M-I) coupling process. It also facilitates the study of the tail when certain features occur in the ionosphere. We examined three states of the magnetotail: pre-onset, substorm expansion, and SMC. All three states are known to have a high occurrence of PBIs and streamers.

2. Methodology

2.1. The OpenGGCM-CTIM-RCM Simulation Model

The OpenGGCM (Open Geospace General Circulation Model) is a global model of the Earth's magnetosphere, ionosphere, and thermosphere. The magnetosphere part solves a set of semi-conservative MHD equations for a single fluid in a 3-D stretched Cartesian grid outside 3 R_E of the Earth (Raeder et al., 2008). The OpenGGCM model simulates auroral emissions by producing the energy flux and mean energy of two populations of precipitating electrons (Raeder, Zhu, et al., 2013). The first population corresponds to the thermal electron flux from the inner magnetosphere forming a diffuse aurora, and the second originates from electrons that have been accelerated in regions of upward FAC forming a discrete aurora (Raeder et al., 2008).

The ionosphere-thermosphere part is based on the Coupled Thermosphere Ionosphere Model (CTIM) that models chemical and photochemical reactions in the upper atmosphere using solar radiation and auroral precipitation as an input (Fuller-Rowell & Codrescu, 1996). A detailed description of the coupling between OpenGGCM and CTIM models can be found in (Raeder, Wang, et al., 2013).

The inner magnetosphere part of the model (ring current) is based on the Rice convection Model (RCM) (Toffoletto et al., 2003), which solves for the motion of plasma flux tubes caused by the ionosphere potential, gradient, and curvature drift. The RCM is coupled via the closure of Region 2 (R2) FACs to the ionosphere and feeds back pressure and density to influence MHD (Cramer et al., 2017).

The model, which is described in greater detail in Raeder et al. (2008), will henceforth be referred to as OpenGGCM. The OpenGGCM model has been used widely to study different magnetospheric phenomena, including substorms and storms (H. K. Connor et al., 2016; Cramer et al., 2017; Ferdousi & Raeder, 2016; Gilson et al., 2012; Raeder, Zhu, et al., 2013), full particle tracing (H. J. Connor et al., 2012; H. K. Connor et al., 2015; Kavosi et al., 2018), responses to shocks (H. K. Connor et al., 2014; Oliveira & Raeder, 2015; Shi et al., 2017), and magnetosphere X-ray imaging (H. K. Connor and Carter, 2019).

2.2. Model Specifications

This study used the Geocentric Solar Ecliptic (GSE) coordinate system throughout the magnetosphere and solar magnetic coordinates in the ionosphere. The numerical simulation box extends from 21 RE in the sunward direction to 500 RE antisunward. The box size in the *YZ* direction (perpendicular to the sun-Earth line) extends from −48 to 48 RE. The model uses non uniform grid resolution with a total of 16×106 grid cells in this simulation. The highest resolution close to the plasma sheet corresponding to a minimum grid cell size of 0.2 R_E. The ionosphere spatial grid resolution of the is 0.5° in latitude and 3° in longitude. The run has started 5 h prior to the substorm onset with 1 h of southward IMF B_z at the beginning of the run to allow for the formation of magnetosphere.

In order to study the relationship between streamers and BBFs, we map different physical parameters, such as the plasma velocity in the X direction and its vorticity $(\nabla \times V)_Z$ from the magnetotail to the ionosphere, after successfully simulating the generation of the propagation of BBFs in the tail. The velocity mapping in the earthward direction is used because it resembles the structure of the BBF and provides insight into the convection structure in the ionosphere moving equatorward. As a bubble moves earthward, the field lines ahead of it are pushed outward and away from the bubbles, leading to vorticity outside the bubble. The vorticity leads to the occurrence of shear and twist of magnetic field lines corresponding to the FAC that maps to the ionosphere (Birn et al., 2004).

The mapping technique is used because the model grid cannot sufficiently resolve the aurora's fine structure near the ionosphere, where the field lines converge. For instance, the FAC generated by the shear of the magnetic field around the plasma bubbles dissipates numerically before reaching the inner boundary of the MHD (2.5 RE). In other words, the structures that fit within five to seven grid cells in the tail occupy one grid cell or less at the inner boundary of the MHD domain and cannot be resolved numerically.

While our model cannot provide fine structure precipitation and auroral emission patterns, we rely on the current understanding of the relationship between the auroral streamers and the convection associated

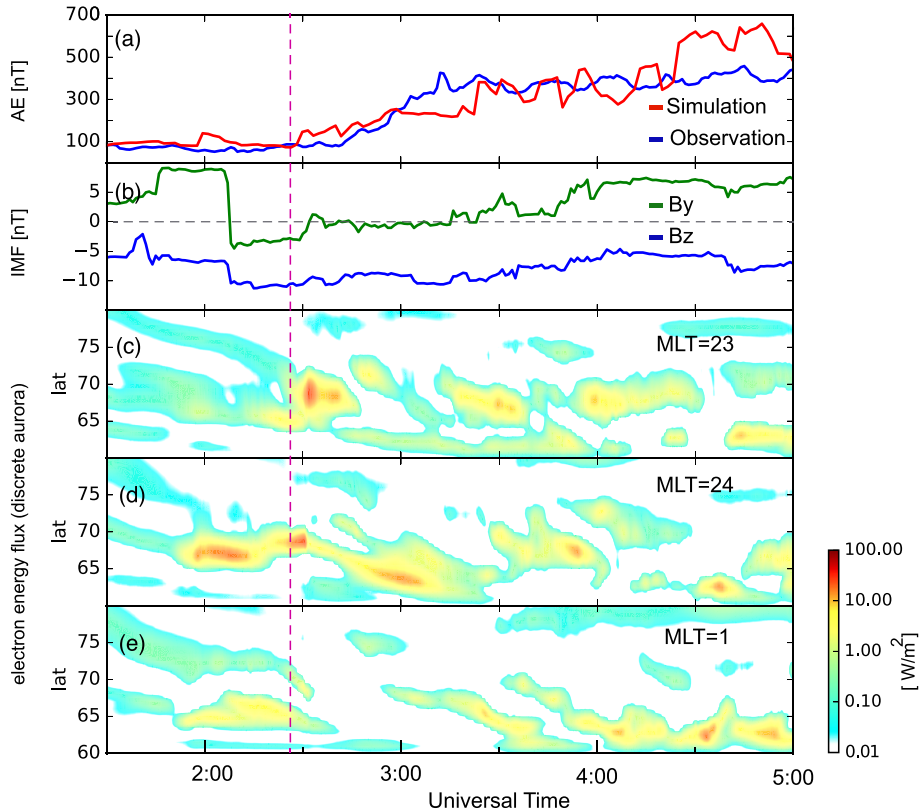

Figure 1. General overview of the January 03, 2001, substorm event. AE index based on simulation and observation, IMF B_z and B_y from OMNI, and discrete aurora from OpenGGCM simulation. The dashed line indicates the substorm onset at 02:28 UT.

with the BBFs, specifically the streamer that is the narrow auroral feature appearing on the duskward edge of the BBF convection pattern (Shi et al., 2017). Our model provides the BBF convection and its ionospheric footpoint, and we assume that the streamer precipitation pattern in the ionosphere would appear on the duskward edge of the mapped convection structure. This assumption is justified as long as the streamer aurora is associated with the upward FAC on the convection structure's duskward edge, irrespective of whether the precipitating electrons are scattered into the loss cone from the source or locally accelerated at lower altitudes. We thus map the tail of the fast flow structures magnetically to the ionosphere.

3. Observations Overview on January 03, 2001

We studied the January 03, 2001, substorm event that was comprehensively studied by Zesta et al. (2006) with several data sets available for comparison. The interplanetary magnetic field (IMF) conditions based on the OMNI are shown in Figure 1b. The IMF B_z is southward for the entire event, while the IMF B_y is mostly positive. The ground auroral observations are shown in Zesta et al. (2006), Figure 1 from the Rankin Inlet meridian scanning photometer (MSP). The first substorm auroral ground signature in the MSP is observed at 0240 UT. However, the MSP was located at a higher latitude than the onset location, and it missed the first onset signature at 0230 UT observed in the ground magnetometers. The MSP shows the auroral signatures in the 6300 $A°$ (mostly diffuse aurora) and 5577 $A°$ (mostly discrete aurora and PBIs) bands, respectively (Figure 1a and 1b of Zesta et al. (2006)). The substorm recovery starts around 0325 UT and, subsequently, transitions to the SMC owing to the continuous southward B_z driver when reconnected on the dayside is balanced by the reconnection on the nightside, and the auroral electrojet (AE) remains constant at ~400 nT 1-b (McWilliams et al., 2008). The Geotail spacecraft was near the center of the plasma sheet during this event, and several fast flows were observed during this time.

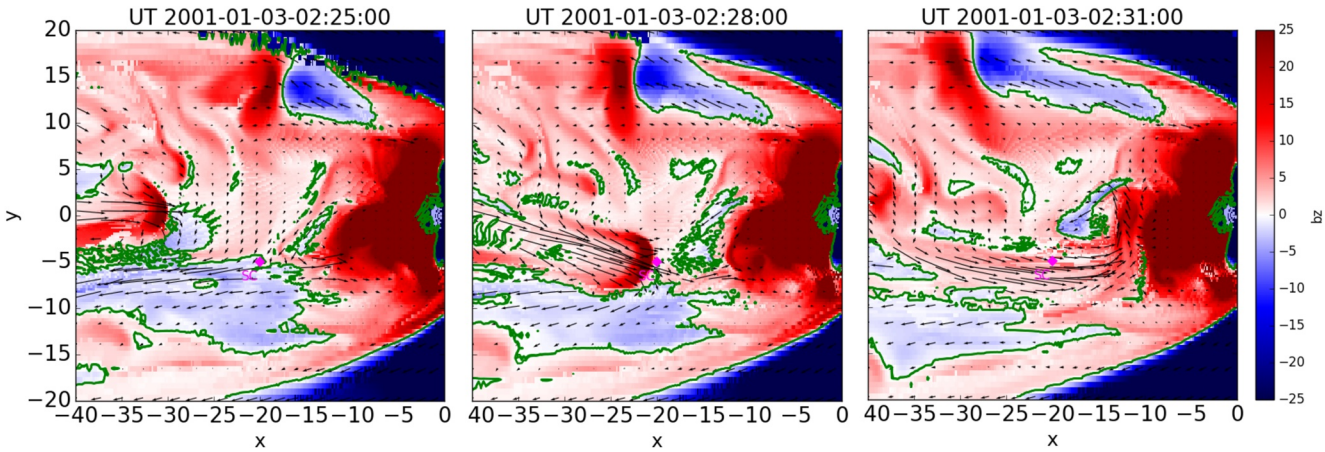

Figure 2. Magnetic field Bz in nT with flow vectors in the central plasma sheet at three different times. The green lines are the contours of Bz = 0. The plots represent the passage of a strong BBF before onset. The magenta diamonds represent the location of the virtual satellite.

4. Simulation Overview on January 03, 2001

4.1. Ionosphere and Aurora

Figure 1 shows the (a) AE index from the observation and simulation, (b) IMF conditions, and (c–e) energy flux of the precipitating electrons at different longitudes (varying from 23 to 1 MLT) as a function of time and magnetic latitude derived from the simulation. Movie S1 shows a simulated diffuse and discrete aurora during this time. Note that model used OMNI solar wind as an input which is shifted by about 55 min, while Zesta et al. (2006) evaluate the events based on ACE shifted 75 min solar wind data. The auroral activity starts around 0158 UT at midnight MLT, but we identify it as pseudo aurora breakup because the auroral oval does not expand, and the simulated AE index slightly increases and goes back to normal because the aurora breakup is very localized. We identify the substorm onset in the model ~0228 UT with the auroral intensification starting at midnight MLT and 68° latitude indicated by the magenta dashed line in Figure 1. Afterward, the intensification propagates equatorward and westward, forming the Westward Traveling Surge (WTS) (Akasofu, 1964; Roux et al., 1991), a typical signature of substorm expansion. While the WTS is most prominent in the discrete aurora (Figure 3), diffuse aurora also intensifies later in the morning sector (Movie S1). The AE index also reaches 200 nT, indicating isolated substorm onset (Angelopoulos et al., 2008). After substorm onset, the aurora in the model remains active until 0500 UT owing to the strong and continuous southward IMF B_z and strong positive IMF B_y. The substorm onset time in the simulation is consistent with the one from observations by (Zesta et al., 2006). The model then transitions to the SMC condition after 0330 UT because the reconnection on the dayside is balanced by reconnection in the nightside with continuous southward IMF B_z (Dejong and Clauer, 2005; Pytte et al., 1978). The SMC mode can also be interpreted from the steadiness of the AE index a couple of hours after a substorm's initiation (Kissinger et al., 2010; McWilliams et al., 2008).

4.2. Magnetotail Dynamics

To better understand the sequence of events in the magnetotail that leads to the onset of the auroral substorm in the model, we further study the configuration of BBFs and dipolarization fronts in the CPS. Figure 2 shows the rendering of the Bz component of the magnetic field in the plasma sheet at three different times in 5-min intervals. The magenta diamond shows the virtual satellites' location at SC1 (x = −20, y = −5). Besides, Movie S2 shows the tail activity during this time, with a resolution of 10 s. Black arrows indicate the flow vectors, while the green lines are the Bz = 0 contours. The plasma sheet center is defined by the condition Bx(z) = 0 (see Raeder et al. (2008) for details). Thus, Movie S2 does not show a plane cut but a projection of the plasma sheet's center.

At 0135 UT, the magnetotail is very quiet, and fast flow and dipolarization activity are limited, even though the IMF Bz is slightly southward. As time progresses, new flow channels begin to form, and several small

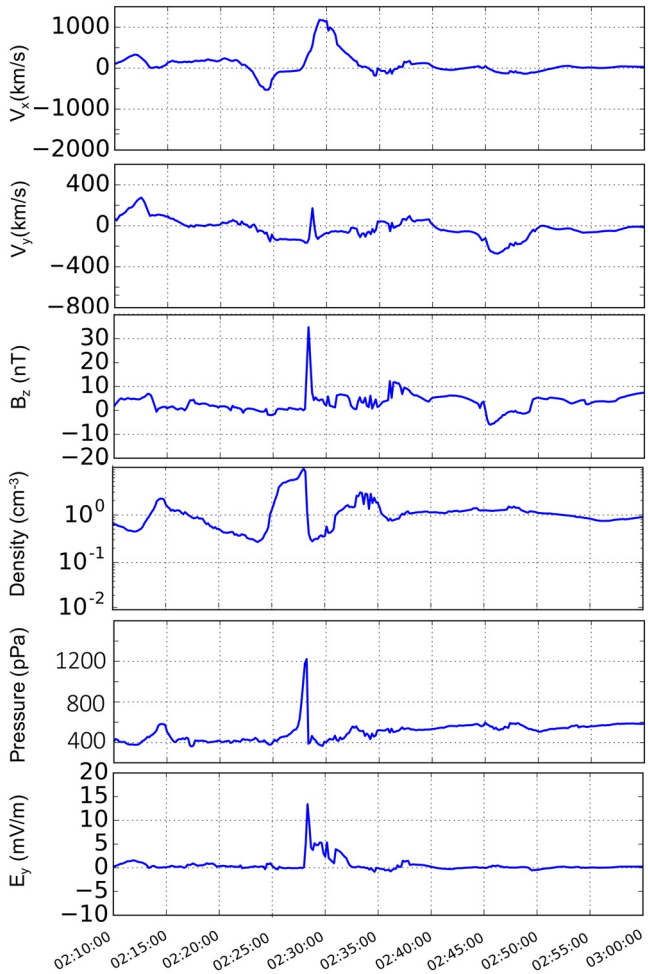

Figure 3. The time series of the flow velocity (Vx and Vy), magnetic field (Bz), density, pressure, and electric field (Ex and Ey) in the plasma sheet at $x = -20$ and $y = -5$ (SC satellite, magenta diamond in Figure 2).

reconnection sites start to appear around 0145 UT when the IMF By turns positive. At 0200 UT, the reconnection sites have expanded and merged, and the resulting x-line is as close as 13 RE from Earth before the first pseudo aurora breakup. The reconnection generates strong flows that move both earthward and tailward. To compare our simulation results with the typical point observations of BBFs, we insert a virtual satellite SC1 ($X = -20$, $Y = -5\ R_E$). Figure 3 shows all the key observed BBF characteristics, that is, a 10 min interval of earthward flows with speeds up to 1000 km/s, large dawnward and duskward flow deflections, rapid field dipolarizations that coincide with the intermittent flow bursts within the BBF, and reduced density and plasma pressure following the dipolarizations. Thus, we refer to these fast flows in the simulation as BBFs. As a result of the earthward flow breaking, diversion, and flow shear, FACs with Region 1 (R1), i.e., substorm current wedge, polarity, are generated, which leads to the rapid intensification of the discrete aurora in the midnight region, as shown in Figure 1. We note that there are several fast flow reconnection sites in the plasma sheet before substorm onset. However, the strongest BBF occurs at 02:28 UT immediately before the substorm onset (Figure 3). Geotail also observed a BBF around the same location ($X = -20.98$ and $Y = -5.79\ R_E$) and same time (~0245 UT) with similar characteristics but lower plasma velocity as shown in Figure 2 of Zesta et al. (2006).

Movie S2 also shows that during the SMC, fast Earthward flows increase, and the activity moves toward the flanks from the midnight region, which is consistent with the statistical study by Kissinger et al. (2012), which showed that the average flux transport is higher in the flanks during SMC conditions. This event can also be characterized as an active SMC with AL index ~ −300 and strong IMF B_z(DeJong, 2014). Overall, this event provides an opportunity to compare our results during three phases: (1) pre-onset, (2) substorm onset and expansion, and (3) SMC phase. However, it is to be noted that no strict demarcation between phases (2) and (3) exists because the SMC is essentially the substorm's extended recovery.

5. Projection of Tail Dynamics to the Ionosphere

We use the OpenGGCM model to map fast flows, similar to Figure 3 to the ionosphere. For the mapping, we used different magnetosphere parameters, including different magnetic field components, plasma pressure and density, vorticity, and different components of velocity. A comparison of these maps with observations showed that the velocity and z component of vorticity that leads to FAC formation closely resemble ionosphere streamers.

Figure 4a shows the plasma sheet in the same projection as Figure 2 during the expansion phase of the substorm. However, the color coding indicates the x-component of earthward flows on a logarithmic scale. Figure 4b shows the projection of the flows on the ionosphere along the magnetic field in a standard polar view from a magnetic latitude of 60° to the pole. The dayside is cut off because no flows of interest map to the dayside. Figure 4c shows the mapping of the vorticity $(\nabla \times V)_Z$ from the magnetotail to the ionosphere. The vorticity, which results from shearing around plasma bubbles, leads to the formation of FACs that close in the ionosphere (Birn et al., 2004). Figure 4d shows the flows' projection, but in a rectangular latitude – MLT projection. We have labeled the corresponding features with blue numbers as a visual guide. The aurora signatures and flows are identified visually. Also, Movie S3, provides more detailed information regarding fast flows and their mapping in the ionosphere during this time with a resolution of 10 s.

The tail flows are regions of strong gradients in the tail. As such, they generate FACs through flow shear, pressure gradients, and inertial currents. FACs, in turn, are necessary for accelerating electrons that cause

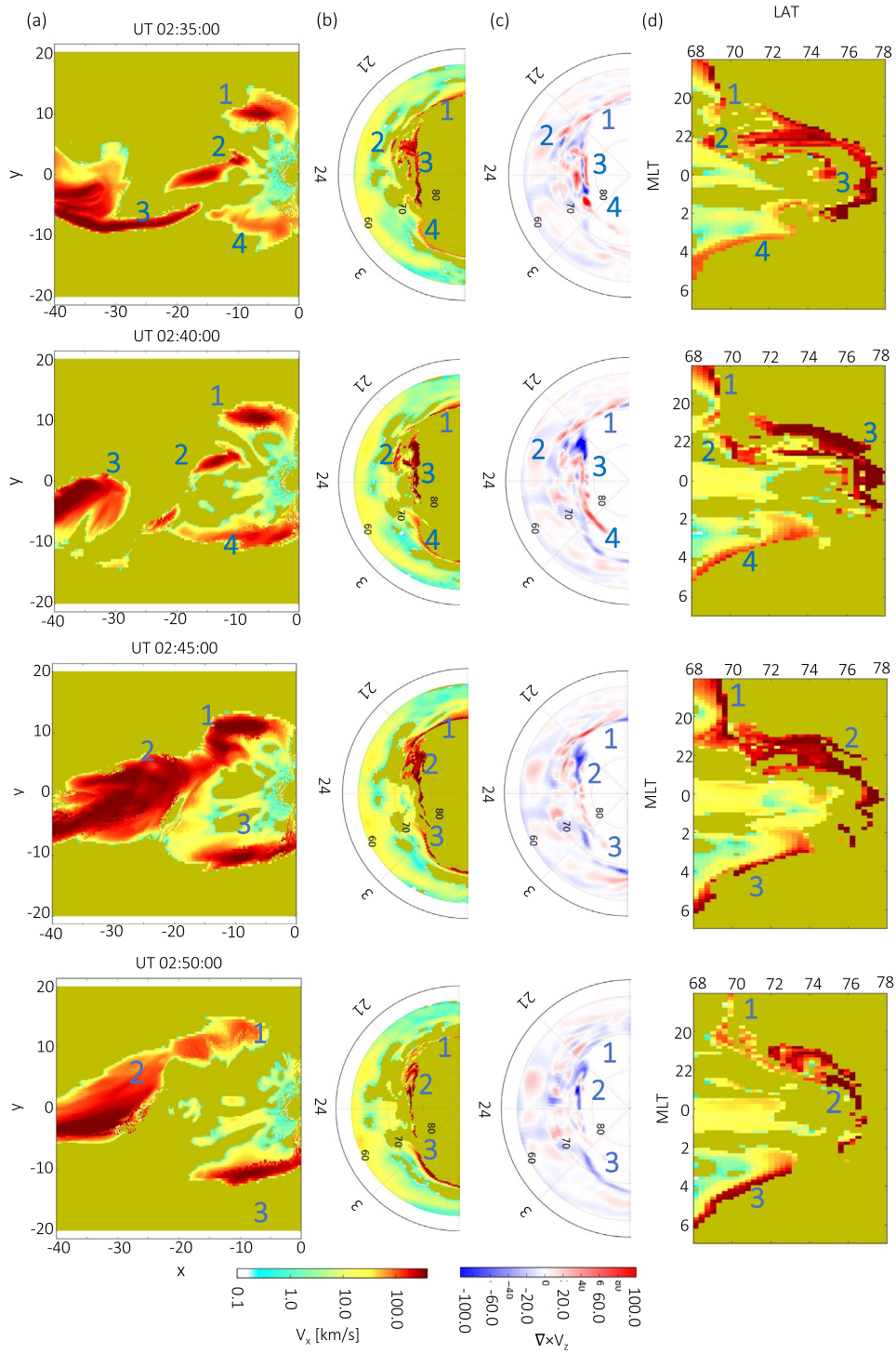

Figure 4. Earthward moving flows in the plasma sheet (a), their projection on the ionosphere polar plot (b), vorticity mapping (c), earthward velocity (d), and before substorm onset. The dotted semicircles indicate magnetic latitudes ranging from 60 to 80. The blue numbers identify flows and their correspondence in the ionosphere.

some of the auroral emissions. Likewise, the flows energize plasma as they impinge on the inner magnetosphere and break, possibly enhancing pitch angle scattering and, thus, diffuse electron precipitation. These processes are modeled self-consistently or using suitable parameterizations to produce the keograms shown in Figure 1. The close correspondence between the flow mapping, keograms, and their comparison with observations (Zesta et al., 2006, Figure 7) suggests that the mapped flows are indeed a good proxy for auroral emissions. They may not indicate their precise locations but properly characterize their dynamic evolution. For this reason we call features in the right two columns of Figures 4 and 5 "auroral features" owing to their resemblance with typical observations.

Based on Movie S3 and Figures 4 and 5, aurora features in the simulation possess the following properties:

- Fast flows in the flanks have more east-west structure in the ionosphere. They are also wider and shorter in longitude and latitude, respectively (Features 1 and 4 in column b)
- Some streamers map to multiple parallel flow channels in the tail (Feature 3 in the first row of Figure 4). These multiple parallel fast flows are similar to previous studies by Zesta et al. (2006), which used the T96 model to map aurora features to the plasma sheet and the Sergeev et al. (1999), their Figure 3
- Each aurora feature is associated with a pair of FAC with opposite polarity (Figure 4c) and their size depends on the dimension of BBFs, which is also consistent with the Birn et al. (2004) study that showed that ionospheric features are associated with FAC
- BBFs do not propagate earthward as straight channels but rather interact with each other and deflect to the other directions. BBFs can also split and merge (Movie S2)
- The streamers (equatorward-moving features) in Figure 5 are the result of the moving and merging of the earthward flows
- At each instance of time, multiple fast flows and reconnection sites can be observed in the plasma sheet consistent with the recent study by McPherron, El-Alaoui, Walker, and Richard (2020)

6. Orientation and Dimension of BBFs and Streamers

We now evaluate the fast flows and aurora feature characteristics during three states of the magnetotail: (1) the pre-onset quiet time, which includes the period between 0130 and 0230 UT, (2) substorm onset and expansion from 0230 to 0330 UT, and (3) SMC phase that starts after 0330 UT and lasts until the end of the run at 0500 UT. Figure 6 shows the number of BBFs during these three stages. Fast flows are identified at the various boundary locations by inward flow velocity values at the magnetic equator that exceed a boundary distance-dependent cutoff value. Due to the rapidly fluctuating nature of the number of fast flows on the nightside at any given time, the count is smoothed over 10-min intervals to provide a better visual of the fast flow activity level. The differently-colored lines represent fast earthward flows at different boundary distances and different cutoffs to account for flow braking as they approach the Earth. The number of fast flows increases during substorm expansion and the SMC. Flows also penetrate closer to the Earth (8–10 R_E) during SMC (blue and green lines in Figure 6).

Zesta et al. (2006), in section 3.2, gives a comprehensive discussion on the dependence of the BBF's orientation on background convection that is partly driven by IMF B_y. They postulate that the fast flows should have dawnward orientation during the January 03, 2001 event due to positive IMF B_y. However, their hypothesis could not be confirmed owing to the limited number of multi-point observations in the magnetotail and the mapping techniques based on T96. We thus perform statistical analyses on 47 BBFs near the Earth ($x \leq -40\ R_E$) and nightside auroral features based on the OpenGGCM simulation result.

Figure 7 shows the kernel density estimation (KDE) for the location and dimension of fast flows during the three phases and for the entire simulation time. BBFs dimension was selected by eye based on Movie S3 in supplement. Fast flows are more likely to be observed closer to the Earth during SMC, in midtail during substorm expansion, and they are closer to the Earth before the substorm onset (Figure 7a). The location of BBFs also depends on the state of the tail or direction of IMF B_y. They are mostly observed at dusk ($y = -5R_E$) during pre-onset when IMF B_y rotates from positive to negative (Figure 1a). During onset and IMF $B_y = 0$, these flows are mainly located in the midnight region. Their most probable location is at dawn ($y = 10R_E$) during SMC and when IMF B_y is positive (Figure 7c). The azimuthal direction of fast flows is determined by using the angle of V_y/V_x shown in Figure 7e. The fast flows azimuthal direction is mostly

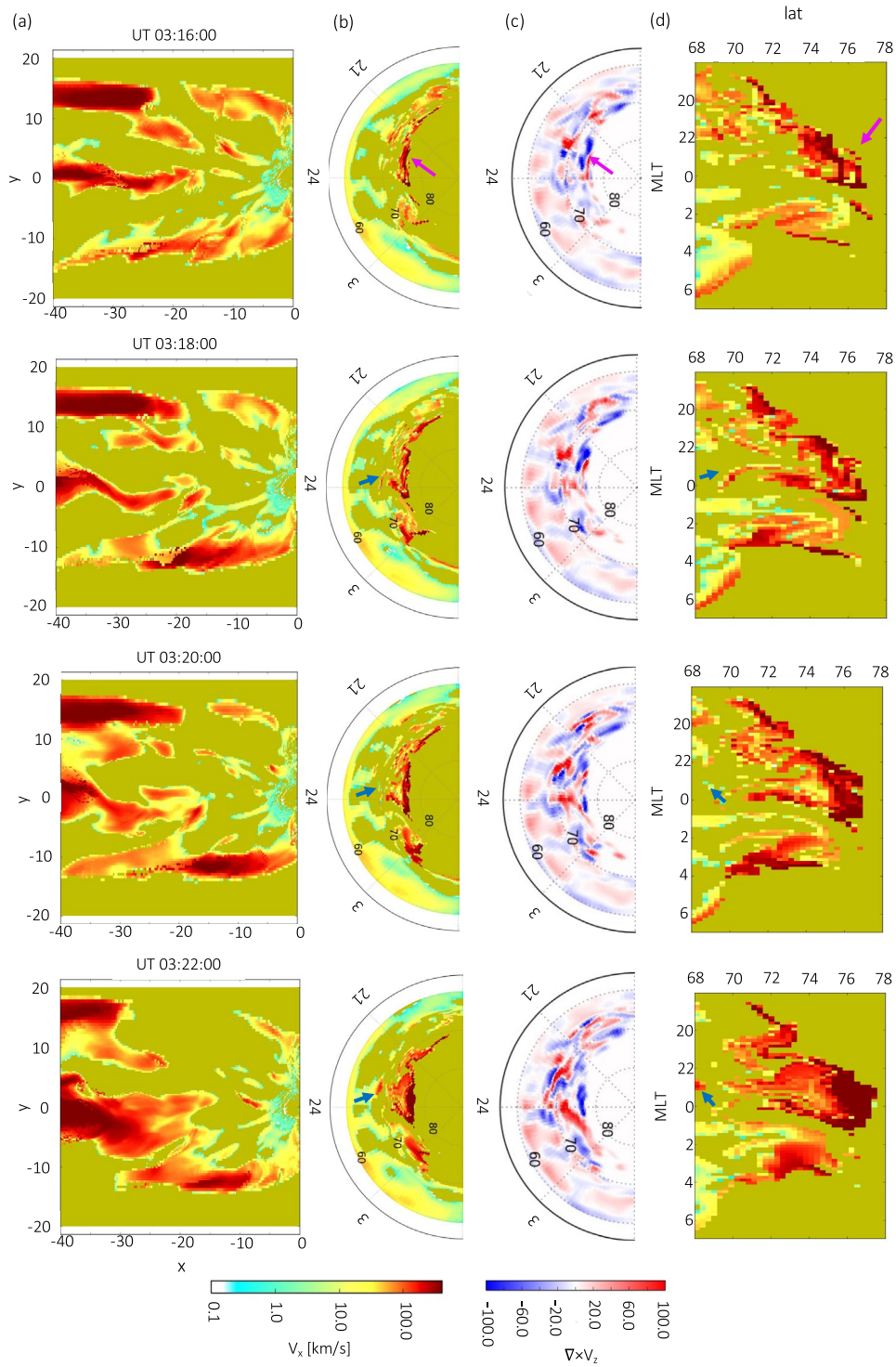

Figure 5. The same format as in Figure 4. The evolution of a PBI during the SMC from 0316 to 0322 UT at intervals of 2 min. The magenta arrow points to the location of the PBIs (77 latitude and 22 MLT) as an intensification in the poleward boundary of the aurora in (a) and (b) row 1. These PBIs then propagate equatorward and dawnward as streamers, as indicated by the blue arrows in the next three panels.

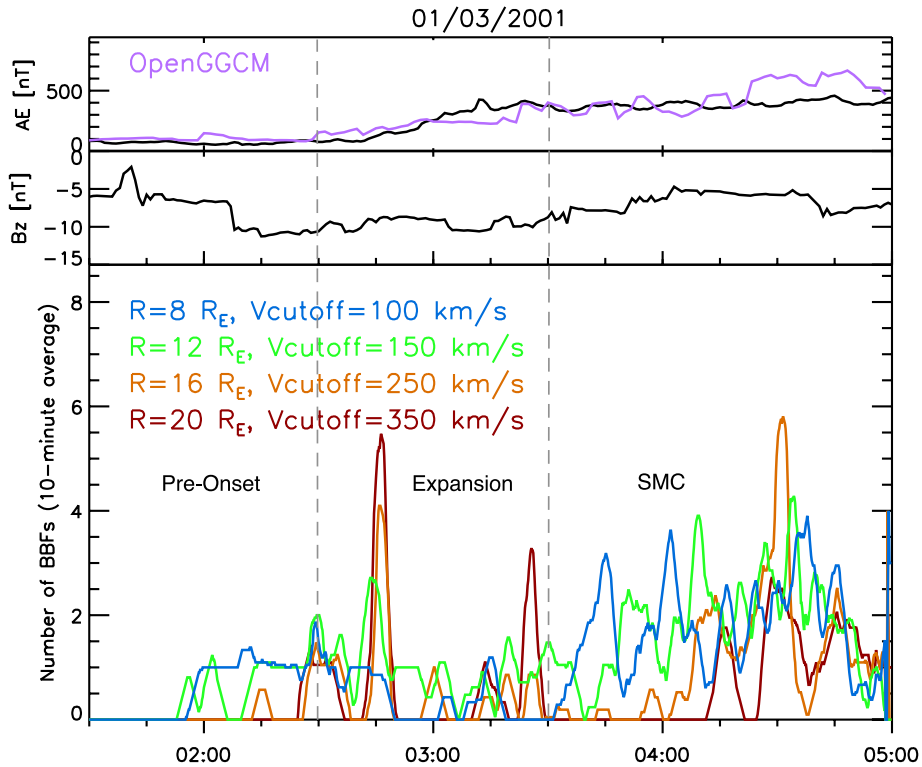

Figure 6. Number of BBFs during different magnetospheric states: before the onset, expansion, and SMC. The colors represent different boundaries in the tail with different velocity cutoffs.

dawnward with a mean angle − 8.6° for all flows, and their direction does not change much during different phases of the magnetotail or IMF B_y direction.

It is not possible to distinguish whether the preference of fast flows in the plasma sheet is driven by the direction of the IMF B_y or the state of the magnetosphere. However, a previous study (Juusola, Østgaard, & Tanskanen, 2011) showed that the azimuthal direction of fast flows depends on the IMF B_y, and they are dawnward and duskward under positive and negative values of IMF B_y, respectively. Our observation is consistent with our analysis that fast flows and streamers are observed at dawn during positive IMF B_y, which confirms the hypothesis by Zesta et al. (2006) (Figure 5). However, mapping streamers to the plasma sheet based on T96 in Zesta et al. (2006) (Figure 7) did not indicate the fast flows' dawnward orientation. Addressing this issue, they suggest that it might originate from the mapping technique because the T96 model is based on averaging magnetic fields and, hence, might not be reliable on highly stretched magnetic fields.

The BBF length scale ranges from 5 to 20 R_E, with the most probable length and mean being $x = 5R_E$ and $x = 11R_E$, respectively. They also do not change much under different conditions (Figure 7b). The widths of BBFs range from 1 to 8 R_E with the most probable width of 2 R_E during the expansion of the substorm and SMC, and 4 R_E before the substorm onset. The sizes of BBFs in the model consistent with (Sharma et al., 2008) studied that are estimated to be around $4 - 40R_E$ and $2 - 4R_E$ in the X and Y directions, respectively.

Figure 8 shows the same statistical distribution for the dimension and location of aurora features based on mapping fast flows along the magnetic field to the ionosphere. Auroral features are observed at higher latitudes ($LAT = 74$) before the onset and are equally observed at $LAT = 70$ and 74 during substorm expansion. However, they are distributed evenly between 68 and 75 during SMC (Figure 8a). Streamer's MLT also changes according to the state of the magnetosphere or direction of IMF B_y (Figure 8b). Their preferred location is at pre-midnight (MLT = 22) before the onset and during the substorm's expansion phase, and their preferred location is in the morning sector (MLT = 1) during SMC conditions. Streamers are shorter

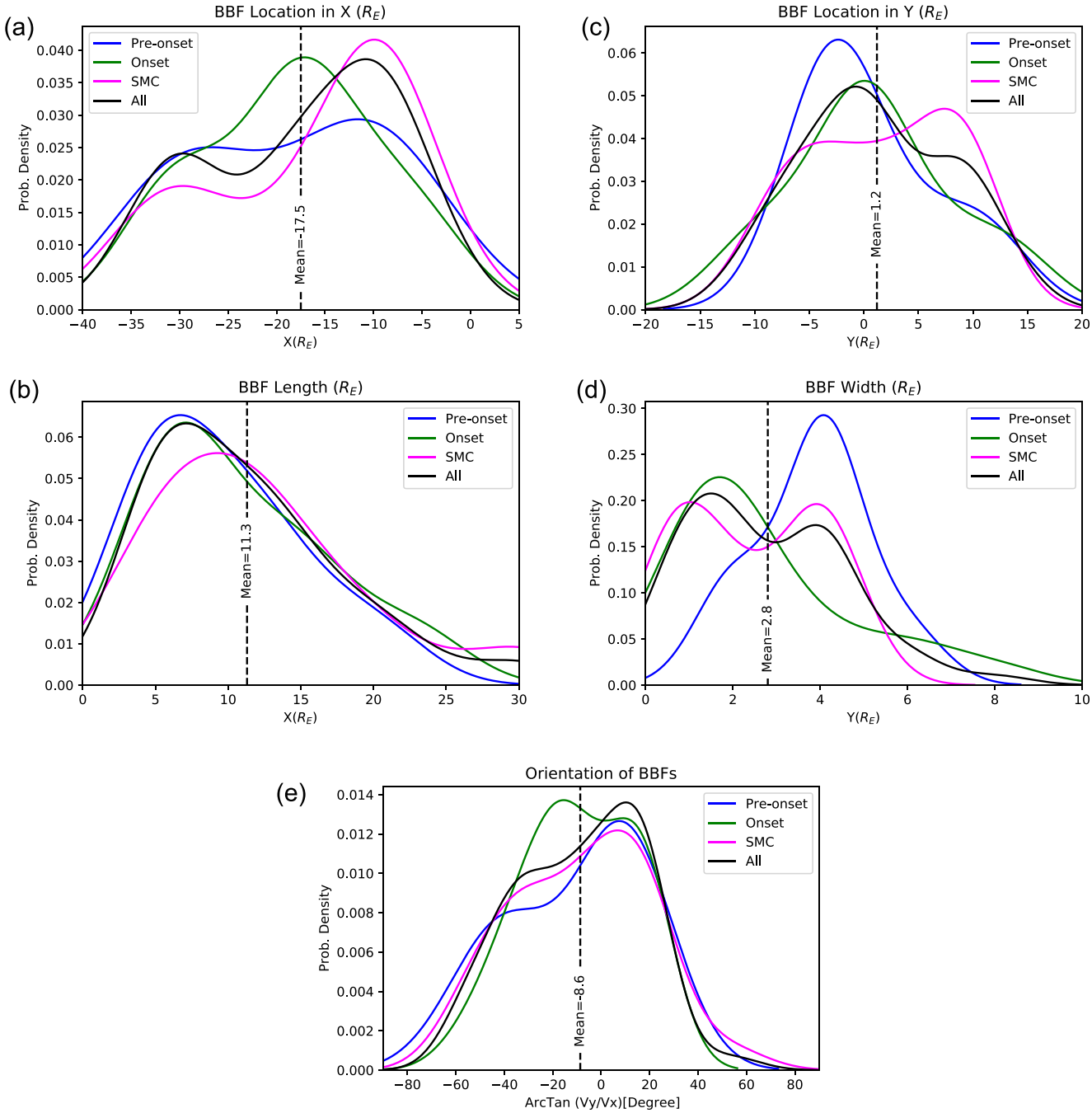

Figure 7. Probability density for the location and dimension of fast flows in the plasma sheet based on 47 individual BBFs in the OpenGGCM simulation.

in latitude (LAT = 2) during expansion and longer during SMC. The streamers width range from 1 to 6° in longitude, with a most probable width of 2° (Figure 8d) similar to Gabrielse et al. (2018) study.

7. Summary and Conclusions

BBFs are a significant component of convection and flux transport in the Earth's magnetosphere. Observationally, it is challenging to study their topology, motion, and overall spatial and temporal structure owing to limited in-situ data coverage. On the other hand, auroral streamers are much easier to observe, and their development can be followed over time with arrays of ground-based imagers. Thus, if streamers represent

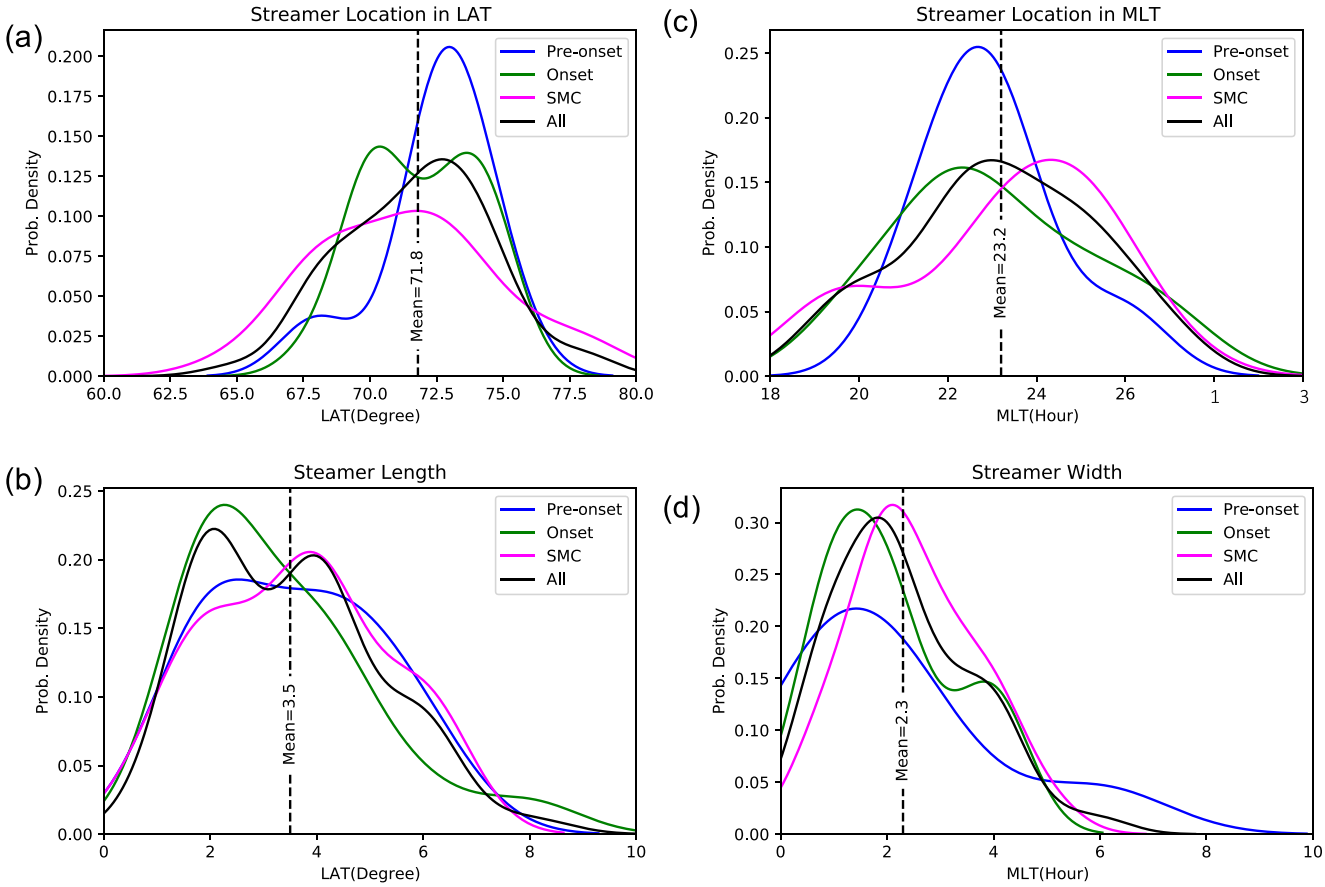

Figure 8. Probability density for the location and dimension of aurora features in the nightside ionosphere based on 47 individual events in the OpenGGCM simulation.

the footpoints on the BBFs in the ionosphere, one can, in principle, study some aspects of BBFs from the ground. Therefore, it is essential to determine the correlation between streamers and BBFs to guide observations. In this study, we used the OpenGGCM model to study that relationship before the onset of a substorm, during the substorm expansion, and subsequently during a SMC interval. We used the substorm event on January 03, 2001, because there are many aurora measurements for this event, providing the opportunity to compare our simulations with observations that were studied comprehensively by Zesta et al. (2006). Our study, which is the first attempt to study the correlation of BBFs and streamers using a physics-based self-consistent global model of the magnetosphere, provides an opportunity for remote sensing of magnetotail dynamics.

By mapping along magnetic field lines in the MHD model, we resolve the fine structure of auroral features in the ionosphere and relate them to the magnetotail's physical processes. We did not consider any specific mechanism that produces the aurora but assume that, whatever the process is, it is bound to follow field lines (Korth et al., 2014). Thus, we cannot make specific assumptions about the precise nature of the auroral precipitation and map the earthward flow velocity and the flow vorticity from the tail to the ionosphere. Depending on the location of the BBF in the tail, and the dynamics of the tail, the aurora streamers develop different signatures in the ionosphere. We summarize the key features below:

1. BBFs do not always move in a straight line, and they interact and merge as they move Earthward, leading to streamers in the ionosphere
2. The number of flow channels and their strength in the plasma sheet increases during substorm expansion and again during the SMC interval. Auroral activities, including PBIs and streamers, are also more abundant after the substorm onset and during SMC

3. Multiple fast flow channels and reconnection sites can be observed at the same time across the plasma sheet
4. The location of BBFs and streamers may depend on the state of the magnetosphere and direction of IMF B_y
   (a) BBFs are mostly detected at dusk, midnight, and dawn during pre-onset (B_y rotates from negative to positive), substorm expansion ($B_y = 0$), and SMC ($B_y \geq 0$). Thus, streamers are observed in the pre-midnight and morning sectors in the nightside ionosphere.
   (b) BBFs are closer to the Earth before the substorm onset, during SMC, and they are observed in mid-tail (~ 20) in the substorm's expansion phase.
   (c) They are deflected mostly toward dusk during this event and their deflection do not change much with direction of IMF B_y or state of the magnetotail.
   (d) Lengths of BBFs features do not depend on the state of the magnetosphere and range between 5 and 20 R_E. However, the width of BBFs is correlated with the magnetospheric state or IMF B_y. They are narrower during substorm expansion and SMC than before onset.

Data Availability Statement

Data from the model simulations used in this study are available online https://zenodo.org/deposit/3552974.

Acknowledgment
This research was supported by the National Aeronautics and Space Administration under grants NAS5-02099 (THEMIS) and NNX15AW16G, the National Science Foundation (NSF) under the grant AGS-1603021, and NSF grant 2109543. K.R.M. was supported by the NSF Grant Number 1602403.

References

Akasofu, S.-I. (1964). The development of the auroral substorm. *Planetary and Space Science*, *12*(4), 273–282. https://doi.org/10.1016/0032-0633(64)90151-5

Angelopoulos, V., Kennel, C. F., Coroniti, F. V., Pellat, R., Kivelson, M. G., et al. (1994). Statistical characteristics of bursty bulk flow events. *Journal of Geophysical Research: Space Physics*, *99*(A11), 21257–21280. https://doi.org/10.1029/94JA01263

Angelopoulos, V., McFadden, J. P., Larson, D., Carlson, C. W., Mende, S. B., Frey, H., et al. (2008). Tail reconnection triggering substorm onset. *Science*, *321*(5891), 931–935. https://doi.org/10.1126/science.1160495

Baumjohann, W., Paschemann, G., & Lühr, H. (1990). Characteristics of high-speed ion flows in the plasma sheet. *Journal of Geophysical Research: Space Physics*, *95*(A4), 3801–3809. https://doi.org/10.1029/ja095ia04p03801

Birn, J., Raeder, J., Wang, Y. L., Wolf, R. A., & Hesse, M. (2004). On the propagation of bubbles in the geomagnetic tail. *Annales Geophysicae*, *22*(5), 1773–1786. https://doi.org/10.5194/angeo-22-1773-2004

Connor, H. J., Raeder, J., & Trattner, K. J. (2012). Dynamic modeling of cusp ion structures. *Journal of Geophysical Research: Space Physics*, *117*(A4). https://doi.org/10.1029/2011JA017203

Connor, H. K., & Carter, J. A. (2019). Exospheric neutral hydrogen density at the nominal 10 re subsolar point deduced from XMM-newton x-ray observations. *Journal of Geophysical Research: Space Physics*, *124*(3), 1612–1624. https://doi.org/10.1029/2018JA026187

Connor, H. K., Raeder, J., Sibeck, D. G., & Trattner, K. J. (2015). Relation between cusp ion structures and dayside reconnection for four IMF clock angles: OpenGGCM-LTPT results. *Journal of Geophysical Research: Space Physics*, *120*(6), 4890–4906. https://doi.org/10.1002/2015ja021156

Connor, H. K., Zesta, E., Fedrizzi, M., Shi, Y., Raeder, J., Codrescu, M. V., & Fuller-Rowell, T. J. (2016). Modeling the ionosphere-thermosphere response to a geomagnetic storm using physics-based magnetospheric energy input: OpenGGCM-CTIM results. *Journal of Space Weather and Space Climate*, *6*, A25. https://doi.org/10.1051/swsc/2016019

Connor, H. K., Zesta, E., Ober, D. M., & Raeder, J. (2014). The relation between transpolar potential and reconnection rates during sudden enhancement of solar wind dynamic pressure: OpenGGCM-CTIM results. *Journal of Geophysical Research: Space Physics*, *119*(5), 3411–3429. https://doi.org/10.1002/2013ja019728

Cramer, W. D., Raeder, J., Toffoletto, F. R., Gilson, M., & Hu, B. (2017). Plasma sheet injections into the inner magnetosphere: Two-way coupled OpenGGCM-RCM model results. *Journal of Geophysical Research: Space Physics*, *122*(5), 5077–5091. https://doi.org/10.1002/2017ja024104

DeJong, A. D. (2014). Steady magnetospheric convection events: How much does steadiness matter? *Journal of Geophysical Research: Space Physics*, *119*(6), 4389–4399. https://doi.org/10.1002/2013ja019220

Dejong, D., & Clauer, C. (2005). Polar UVI images to study steady magnetospheric convection events: Initial results. *Geophysical Research*, *32*. https://doi.org/10.1029/2005GL024498

Fairfield, D. H., Mukai, T., Brittnacher, M., Reeves, G. D., Kokubun, S., Parks, G. K., Nagai, T., et al. (1999). Earthward flow bursts in the inner magnetotail and their relation to auroral brightenings, akr intensifications, geosynchronous particle injections and magnetic activity. *Journal of Geophysical Research: Space Physics*, *104*(A1), 355–370. https://doi.org/10.1029/98ja02661

Ferdousi, B., & Raeder, J. (2016). Signal propagation time from the magnetotail to the ionosphere: OpenGGCM simulation. *Journal of Geophysical Research: Space Physics*, *121*(7), 6549–6561. https://doi.org/10.1002/2016ja022445

Frey, H. U. (2010). Comment on "Substorm triggering by new plasma intrusion: Themis all-sky imager observations" by Y. Nishimura et al. *Journal of Geophysical Research: Space Physics*, *115*(A12). https://doi.org/10.1029/2010ja016113

Fuller-Rowell, D. R. S. Q. R. M. T., & Codrescu, M. (1996). A coupled thermosphere-ionosphere model (CTIM). *STEP Report*, *239*(4).

Gabrielse, C., Nishimura, Y., Lyons, L., Gallardo-Lacourt, B., Deng, Y., & Donovan, E. (2018). Statistical properties of mesoscale plasma flows in the nightside high-latitude ionosphere. *Journal of Geophysical Research: Space Physics*, *123*(8), 6798–6820. https://doi.org/10.1029/2018ja025440

Gallardo-Lacourt, B., Nishimura, Y., Lyons, L. R., Zou, S., Angelopoulos, V., Donovan, E., McWilliams, K. A., et al. (2014). Coordinated superdarn themis asi observations of mesoscale flow bursts associated with auroral streamers. *Journal of Geophysical Research: Space Physics*, *119*(1), 142–150. https://doi.org/10.1002/2013ja019245

Gilson, M. L., Raeder, J., Donovan, E., Ge, Y. S., & Kepko, L. (2012). Global simulation of proton precipitation due to field line curvature during substorms. *Journal of Geophysical Research: Space Physics*, *117*(A5). https://doi.org/10.1029/2012ja017562

Henderson, M. G., Reeves, G. D., & Murphree, J. S. (1998). Are north-south aligned auroral structures an ionospheric manifestation of bursty bulk flows? *Geophysical Research Letters*, *25*(19), 3737–3740. https://doi.org/10.1029/98gl02692

Ieda, A., Machida, S., Mukai, T., Saito, Y., Yamamoto, T., Nishida, A., et al. (1998). Statistical analysis of the plasmoid evolution with geotail observations. *Journal of Geophysical Research: Space Physics*, *103*(A3), 4453–4465. https://doi.org/10.1029/97ja03240

Juusola, L., Østgaard, N., Tanskanen, E., Partamies, N., & Snekvik, K. (2011). Earthward plasma sheet flows during substorm phases. *Journal of Geophysical Research: Space Physics*, *116*(A10), a, n. https://doi.org/10.1029/2011JA016852

Juusola, L., Østgaard, N., & Tanskanen, E. (2011). Statistics of plasma sheet convection. *Journal of Geophysical Research: Space Physics*, *116*(A8). https://doi.org/10.1029/2011ja016479

Kauristie, K., Sergeev, V. A., Kubyshkina, M., Pulkkinen, T. I., Angelopoulos, V., Phan, T., et al. (2000). Ionospheric current signatures of transient plasma sheet flows. *Journal of Geophysical Research: Space Physics*, *105*(A5), 10677–10690. https://doi.org/10.1029/1999ja900487

Kavosi, S., Spence, H., Fennell, J., Turner, D., Connor, H., & Raeder, J. (2018). MMS/FEEPS observations of electron microinjections due to kelvin-helmholtz waves and flux transfer events: A case study. *Journal of Geophysical Research: Space Physics*, *123*, 5364, 5378. https://doi.org/10.1029/2018JA025244

Keiling, A., Angelopoulos, V., Runov, A., Weygand, J., Apatenkov, S. V., Mende, S., et al. (2009). Substorm current wedge driven by plasma flow vortices: Themis observations. *Journal of Geophysical Research: Space Physics*, *114*(A1). https://doi.org/10.1029/2009ja014114

Kepko, L., Spanswick, E., Angelopoulos, V., Donovan, E., McFadden, J., Glassmeier, K.-H., et al. (2009). Equatorward moving auroral signatures of a flow burst observed prior to auroral onset. *Geophysical Research Letters*, *36*(24). https://doi.org/10.1029/2009gl041476

Kissinger, J., McPherron, R. L., Angelopoulos, V., Hsu, T.-S., & McFadden, J. P. (2010). An investigation of the association between steady magnetospheric convection and cir stream interfaces. *Geophysical Research Letters*, *37*(4). https://doi.org/10.1029/2009gl041541

Kissinger, J., McPherron, R. L., Hsu, T.-S., & Angelopoulos, V. (2012). Diversion of plasma due to high pressure in the inner magnetosphere during steady magnetospheric convection. *Journal of Geophysical Research: Space Physics*, *117*(A5). https://doi.org/10.1029/2012ja017579

Korth, H., Zhang, Y., Anderson, B. J., Sotirelis, T., & Waters, C. L. (2014). Statistical relationship between large-scale upward field-aligned currents and electron precipitation. *Journal of Geophysical Research: Space Physics*, *119*(8), 6715–6731. https://doi.org/10.1002/2014ja019961

Liang, J., Ni, B., Spanswick, E., Kubyshkina, M., Donovan, E. F., Uritsky, V. M., et al. (2011). Fast earthward flows, electron cyclotron harmonic waves, and diffuse auroras: Conjunctive observations and a synthesized scenario. *Journal of Geophysical Research: Space Physics*, *116*(A12), a, n. https://doi.org/10.1029/2011JA017094

Lyons, L. R., Nishimura, Y., Shi, Y., Zou, S., Kim, H.-J., Angelopoulos, V., et al. (2010). Substorm triggering by new plasma intrusion: Incoherent-scatter radar observations. *Journal of Geophysical Research: Space Physics*, *115*(A7). https://doi.org/10.1029/2009ja015168

McPherron, R. L., El-Alaoui, M., Walker, R. J., Nishimura, Y., & Weygand, J. M. (2020). The relation of n-s auroral streamers to auroral expansion. *Journal of Geophysical Research: Space Physics*, *125*(4), e2019JA027063. https://doi.org/10.1029/2019JA027063

McPherron, R. L., El-Alaoui, M., Walker, R. J., & Richard, R. (2020). Characteristics of reconnection sites and fast flow channels in an MHD simulation. *Journal of Geophysical Research: Space Physics*, *125*(9), e2019JA027701. https://doi.org/10.1029/2019JA027701

McWilliams, K. A., Pfeifer, J. B., & McPherron, R. L. (2008). Steady magnetospheric convection selection criteria: Implications of global superdarn convection measurements. *Geophysical Research Letters*, *35*(9). https://doi.org/10.1029/2008gl033671

Mella, M. R., Lynch, K. A., Hampton, D. L., Dahlgren, H., Kintner, P. M., Lessard, M., et al. (2011). Sounding rocket study of two sequential auroral poleward boundary intensifications. *Journal of Geophysical Research: Space Physics*, *116*(A1). https://doi.org/10.1029/2011ja016428

Mende, S. B., Frey, H. U., Angelopoulos, V., & Nishimura, Y. (2011). Substorm triggering by poleward boundary intensification and related equatorward propagation. *Journal of Geophysical Research: Space Physics*, *116*(A5). https://doi.org/10.1029/2010ja015733

Nishimura, Y., Lyons, L., Zou, S., Angelopoulos, V., & Mende, S. (2010). Substorm triggering by new plasma intrusion: Themis all-sky imager observations. *Journal of Geophysical Research: Space Physics*, *115*(A7). https://doi.org/10.1029/2009ja015166

Oliveira, D. M., & Raeder, J. (2015). Impact angle control of interplanetary shock geoeffectiveness: A statistical study. *Journal of Geophysical Research: Space Physics*, *120*(6), 4313–4323. https://doi.org/10.1002/2015ja021147

Pitkänen, T., Hamrin, M., Norqvist, P., Karlsson, T., & Nilsson, H. (2013). IMF dependence of the azimuthal direction of earthward magnetotail fast flows. *Geophysical Research Letters*, *40*(21), 5598–5604. https://doi.org/10.1002/2013gl058136

Pitkänen, T., Kullen, A., Laundal, K. M., Tenfjord, P., Shi, Q. Q., Park, J.-S., et al. (2019). IMF by influence on magnetospheric convection in earth's magnetotail plasma sheet. *Geophysical Research Letters*, *46*(21), 11698–11708. https://doi.org/10.1029/2019gl084190

Pitkänen, T., Kullen, A., Shi, Q. Q., Hamrin, M., De Spiegeleer, A., & Nishimura, Y. (2018). Convection electric field and plasma convection in a twisted magnetotail: A themis case study 1–2 January 2009. *Journal of Geophysical Research: Space Physics*, *123*(9), 7486–7497. https://doi.org/10.1029/2018ja025688

Pontius Jr, D. H., & Wolf, R. A. (1990). Transient flux tubes in the terrestrial magnetosphere. *Geophysical Research Letters*, *17*(1), 49–52. https://doi.org/10.1029/gl017i001p00049

Pytte, T., McPherron, R. L., Hones Jr, E. W., & West Jr, H. I. (1978). Multiple-satellite studies of magnetospheric substorms: Distinction between polar magnetic substorms and convection-driven negative bays. *Journal of Geophysical Research: Space Physics*, *83*(A2), 663–679. https://doi.org/10.1029/ja083ia02p00663

Raeder, J., Larson, D., Li, W., Kepko, L., & Fuller-Rowell, T. (2008). OpenGGCM simulations for the themis mission. *Space Science Reviews*, *141*, 535–555. https://doi.org/10.1007/s11214-008-9421-5

Raeder, J., Wang, Y., & Fuller-Rowell, T. J. (2013). Geomagnetic storm simulation with a coupled magnetosphere-ionosphere-thermosphere model. In *Space weather*. American Geophysical Union (AGU), 377, 384. https://doi.org/10.1029/GM125p0377

Raeder, J., Zhu, P., Ge, Y., & Siscoe, G. (2013). Auroral signatures of ballooning mode near substorm onset: Open geospace general circulation model simulations. In *Auroral phenomenology and magnetospheric processes: Earth and other planets*. American Geophysical Union (AGU), 389, 396. https://doi.org/10.1029/2011GM001200

Roux, A., Perraut, S., Robert, P., Morane, A., Pedersen, A., Korth, A., et al. (1991). Plasma sheet instability related to the westward traveling surge, *Journal of Geophysical Research*, *96*(A10), 17697–17714. https://doi.org/10.1029/91JA01106

Sergeev, V. A., Liou, K., Newell, P., Ohtani, S., Hairston, M., & Rich, F. (2004). Auroral streamers: Characteristics of associated precipitation,convection and field-aligned currents. *Annales Geophysicae*, *22*(2), 537–548. https://doi.org/10.5194/angeo-22-537-2004

Sergeev, V. A., Liou, K., Meng, C. I., Newell, P. T., Brittnacher, M., Parks, G., & Reeves, G. D. (1999). Development of auroral streamers in association with localized impulsive injections to the inner magnetotail. *Geophysical Research Letters*, *26*(3), 417–420. https://doi.org/10.1029/1998gl900311

Sharma, A. S., Nakamura, R., Runov, A., Grigorenko, E. E., Hasegawa, H., Hoshino, M., Louarn, P., et al. (2008). Transient and localized processes in the magnetotail: A review. *Annales Geophysicae*, *26*(4), 955–1006. https://doi.org/10.5194/angeo-26-955-2008

Shi, Y., Zesta, E., Connor, H. K., Su, Y.-J., Sutton, E. K., Huang, C. Y., et al. (2017). High-latitude thermosphere neutral density response to solar wind dynamic pressure enhancement. *Journal of Geophysical Research: Space Physics*, *122*(11), 11559–11578. https://doi.org/10.1002/2017JA023889

Toffoletto, F., Sazykin, S., Spiro, R., & Wolf, R. (2003). Inner magnetospheric modeling with the rice convection model. *Space Science Reviews*, *107*, 175–196. https://doi.org/10.1007/978-94-007-1069-6_19

Tsyganenko, N. A. (1996). Effects of the solar wind conditions in the global magnetospheric configurations as deduced from data-based field models (Invited)., 389, 181.

Zesta, E., Lyons, L., Wang, C.-P., Donovan, E., Frey, H., & Nagai, T. (2006). Auroral poleward boundary intensifications (PBIS): Their two-dimensional structure and associated dynamics in the plasma sheet. *Journal of Geophysical Research: Space Physics*, *111*(A5). https://doi.org/10.1029/2004ja010640

Zesta, E., Lyons, L. R., & Donovan, E. (2000). The auroral signature of earthward flow bursts observed in the magnetotail. *Geophysical Research Letters*, *27*(20), 3241–3244. https://doi.org/10.1029/2000gl000027

Zesta, E., Shi, Y., Donovan, E., Spanswick, E., Lyons, L. R., Angelopoulos, V., et al. (2011). Ionospheric convection signatures of tail fast flows during substorms and poleward boundary intensifications (PBI). *Geophysical Research Letters*, *38*(8), a, n. https://doi.org/10.1029/2011GL046758